Cavitation During Deformation of Polymers on the Example of Polypropylene

Andrzej Pawlak

Centre of Molecular and Macromolecular Studies, Polish Academy of Sciences, Sienkiewicza 112, 90-363 Lodz, Poland

Received 30 November 2011; accepted 30 November 2011
DOI 10.1002/app.36565
Published online in Wiley Online Library (wileyonlinelibrary.com).

ABSTRACT: Cavitation during uniaxial deformation of isotactic polypropylene (PP) was studied in samples having different amounts of α and β crystals. It has been shown that deformation is always accompanied by neck formation. Because the very beginning the plastic deformation is accompanied by cavitation. The scale of cavitation, determined with the use of X-ray scattering and volume measurements increases with an increase of the content of β phase in the examined samples. Cavities change their shape with deformation—at first they are elongated perpendicularly to the direction of stretching, next, at the strain of 1.5, they reorient in the direction of deformation, which is connected with changes in the surrounding lamellar structure. The calculations of Guinier's radius showed that two populations of voids are present in deformed PP samples, characterized by the gyration radii of 5 and 13 nm for small deformations. Estimations based on the volume increase and sizes of cavities indicate that typically more than one cavity are present in amorphous layers adhering to lamella surfaces. © 2012 Wiley Periodicals, Inc. J Appl Polym Sci 000: 000–000, 2012

Key words: polypropylene (PP); SAXS; mechanical properties; plastic deformation; cavitation

INTRODUCTION

There are several allotropic modifications of the crystalline structure in isotactic polypropylene (PP). The most common and the most stable is the monoclinic α form. This form is characterized by the "cross-hatched" lamellar morphology, in which radial and tangential lamella coexist. The second possible form, β, is thermodynamically and mechanically less stable than α form. The crystals of trigonal β form grow faster than those of α form; spherulites of β PP exhibit exclusively radial lamellar arrangement. The third possible form, triclinic γ, only occurs in specific conditions of crystallization—at high pressure or during shear flow. The smectic form of PP, which is commonly obtained by quenching of a thin film from the molten state down to the temperature 0–40°C, can be regarded as a "frozen in" intermediate state of order in the crystallization pathway.[1] The smectic form, otherwise known as the mesomorphic state, consists of parallel chains exhibiting a high degree of ordering in their longitudinal arrangement, yet lacking crystallographic register in their lateral packing.

PP with higher contents of β phase may be obtained through crystallization from melt with the use of nucleating agents. The effectiveness of nucleation depends on the crystallization conditions. For instance, it was observed that if injection molding was the processing method, the fraction, *K*, of β crystallites increased with the higher temperature of mold.[2]

α and β crystallographic forms exhibit similarity in behavior in a tensile test. After reaching the yield point, deformation localizes and a neck is formed. Irrespective of a similar character of a tensile test, along with the variations in the crystallographic structure of PP forms, the significant differences in the values of mechanical parameters were noted. The toughness of β form is considerably higher than of α-form. Young's modulus and yield stress decrease with the content of β phase, but elongation to break increases.[3] Direct scanning electron microscopy observations of spherulites' deformation show that lamellae in β-spherulites are able to slide over one another.[4]

The factor which differentiate micro deformation in PP crystallographic forms is the capability of β phase to transform into another phase. It was stated, for instance, that β crystals may transform into α crystals during solid-state drawing. The overall crystallinity is retained during such transformation.[5] Li et al.[6] observed that the β to α transformation is localized in the neck region. The degree of conversion depended on the strain and was nearly 100% for the engineering strain of 230%. The overall crystallinity in their samples was nearly constant for engineering strain below 100% and then slowly decreased (from 59% to 51%) for larger strains.

Correspondence to: A. Pawlak (apawlak@cbmm.lodz.pl).
Contract grant sponsor: MNiSW; contract grant number: N N508 468834.

Riekel and Karger-Kocsis[7] reported that α/β ratio increases during deformation. They also observed the existence of an almost pure, conformationally disordered (condis) phase at the edge of the deformed region, exhibiting highly oriented fiber type wide angle X-ray scattering (WAXS) diffraction pattern. Transition β to α is not the only possibility in drawn PP. Shi et al.[5] claimed that the β form transforms into a smectic form if the drawing temperature is below 80°C, however transformation to a more stable α form occurs if the temperature is higher.

Chu et al.[8] observed that the β form specimens became opaque when stretched in temperatures below 120°C, whereas the α specimens tested at the same conditions remain partially transparent. The reason for the transparency loss in β form was microvoiding, caused according to the authors by a volume contraction during the β → α or β → smectic transformation. The crystal density of the β form (0.921 g/cm^3) is significantly lower than for the α form (0.936 g/cm^3).[8]

Lezak et al.[9,10] investigated the evolution of the crystalline texture and lamellar orientation of β-form PP in the plane-strain compression test. The most important mechanism of plastic deformation in their experiment was an interlamellar slip operating in amorphous layers. This slip mechanism resulted in numerous fine deformation bands, formed due to localization of deformation and acting crystallographic slip systems, including (110) [001] chain slip and (110) [1–10] transverse slip. Shear within deformation bands at the room temperature led to β → smectic phase transformation. The observed concentration of the newly formed smectic phase was 19 wt % at the true strain of 1.49. Another deformation mechanism was the cooperative kinking of lamellae, leading to their reorientation and formation of a chevron-like lamellar arrangement. The authors observed that at the higher strains (i.e., true strains above 1.0) an advanced crystallographic slip and high stretch of amorphous material, as a result of interlamellar shear, caused further intensive fragmentation of lamellar crystals, earlier partially fragmented by deformation bands. The fragmentation was followed by a fast rotation of small unconstrained crystallites with the chain axis toward the flow direction. This leads to the final texture with polymer chains in crystalline and smectic phase oriented toward the free direction of deformation.

The above discussed micromechanisms play an important role also during uniaxial stretching of PP forms. The new factor is the possibility of cavitation.[11–13] Cavities were observed in many semicrystalline polymers tensily deformed at the temperatures above glass transition temperature.[14–16] The previous studies of cavitation in PP were focused on polymers with spherulitic structure, in which α form dominated and β spherulites were incidental.[17] Because the process of cavitation depends on the morphology, we may expect that the differences between crystallographic forms existing on the lamellar and spherulitic level of structure can modify the cavitational behavior.

There is a lot of data on plastic deformation and cavitation in PP,[11–13,17] however cavitation present in PP containing different crystallographic forms was not the subject of detailed studies. As it is known, voids are formed during stretching PP samples, rich in α form crystals. During deformation cavities are usually first observed near the yield point.[11] Voids in a polymer are of a nanometer size, detected by small-angle X-ray scattering, and of micrometer size, visible by microscopy or with the naked eye as a whitening of a polymer. The requirement for cavitation is that the stress initiating plastic deformation of crystals is larger than the resistance to cavitate of amorphous phase. This happens when crystals are thick, with a small number of defects.

The phenomenon of cavitation is not only characteristic of PP containing α phase, but also of PP containing β form. The differences in cavitational behavior of PP containing different crystallographic forms may be expected, resulting, e.g., from the structure of spherulites. It is known that lamellae in β type spherulites have a radial organization, but in α form also tangential lamellae are present. Moreover, transformation of β crystals into α or smectic form is possible, which may also influence the cavitation process. The aim of the studies was to compare the cavitation process during deformation of PP containing different amount of α and β forms.

EXPERIMENTAL

Materials and methods

The material used in the investigation was isotactic PP Malen P, F 401 [$M_w = 297{,}200$, $M_n = 56{,}400$ g/mol, MFR 3 g/10 min (at 190°C, 2.16 kg)], delivered by Basell Orlen Polyolefins. The β phase nucleating agent was calcium salt of pimelic acid.[9] The nucleant in the form of powder was mixed with molten PP using Plasticoder mixer (Brabender). The temperature of mixing was 200°C and the content of pimelic acid salt was 0.2 wt %. Nucleated polymer was pelletized after mixing. The PP granules were melted at the temperature of 190°C and compressed into 1 mm thick plates. The plates were cooled in air or in water with ice, so as to obtain different thermal history, which may influence the crystalline structure and cavitational behavior. One could expect formation of cavities in the samples cooled in air, but probably not in those cooled in iced water, because stronger crystals are

formed when the nonisothermal crystallization process is slower. Apart from these compositions also plates from non-nucleated Malen P were prepared, cooled in air, so as to obtain a material with a dominating α form.

The samples for mechanical test were cut out from the plates, their shape being according to ASTM D638 standard. The gauge zone had initial dimensions of 9.5 mm × 3.18 mm × 1 mm. Mechanical properties were studied at the room temperature using "Instron 5582" tensile machine. Five samples of each kind were tested and results were averaged. The rate of deformation was 5%/min (i.e., 8.3×10^{-4} s^{-1}). Black marks, separated by 1 mm distances, were introduced onto the surfaces of specimens. The marks enabled observation of the local strain during stretching. The changes in the distances between marks were registered using "Canon D50" digital photo camera. The mirror was mounted for observation and recording the third dimension of the sample, i.e., thickness. The actual cross-section and the local strain were calculated on the basis of these dimensions. The local strain was defined as:

$$\varepsilon = (l - l_o)/l_o \tag{1}$$

where l_o is the initial distance between black marks, l – a distance in the deformed sample. The use of local strain in description is alternative to true strain, however it seems that it is easier to compare results presented in the form of local strain than using logarithmic form of the true strain.

Similarly, the volume strain w was defined as:

$$w = (V - V_o)/V_o, \tag{2}$$

where V is the actual volume and V_o is the initial volume, both determined from the width, thickness, and distance between black marks. True stress was determined from measured values of force and actual cross-section.

The deformation process was being stopped at selected strains and the samples after stress release were analyzed by X-ray scattering methods. The presence of cavities and a long period of structure were determined by small angle X-ray scattering (SAXS). A 0.5 m long Kiessig-type SAXS camera was equipped with a pinhole collimator, with the beam size in sample plane of 0.3 mm, and a Fuji imaging plate as a recording medium. The camera was coupled to a Philips PW 1830 X-ray generator (CuK_α, operating at 50 kV and 35 mA) consisting of a capillary collimator, allowing for resolution of scattering objects up to 40 nm. Exposed imaging plates were read with a Phosphor Imager SI system (Molecular Dynamics). A large increase (10 times and more) of scattering intensity was the evidence of cavitation. If the concentration of cavities is small and they are dispersed in the polymer matrix, it is possible to determine the radius of gyration R from the Guinier's equation[18]:

$$I(s) = I_o \rho^2 v^2 \ \exp\ (-4\pi^2 s^2 R^2/3) \tag{3}$$

where I – intensity of scattering, I_o – initial intensity, ρ – difference of electron density between the void and matrix, v – volume of scattering objects, s – scattering vector, and R – gyration radius.

The gyration radius is the measure of size of scattering objects. If these objects are randomly oriented, then R does not depend on the direction of measurements and may be used for determination of the cavities' size. Often in a polymer there exist many groups of cavities of different sizes; then, the Guinier equation has the form:

$$I(s) = I_o \rho^2 \sum_{i=1}^{N} {v_i}^2 \ \exp\ (-4\pi^2 s^2 {R_i}^2/3) \tag{4}$$

where N is the number of cavity group, v_i is the volume of voids in the i-th group, s – scattering vector, R_i – gyration radius for i-th group. The details of R determination for many populations of voids existing in a polymer were described by Yamashita and Nabeshima.[19]

If one of the void's dimensions is larger than the detection range, in our experiment 40 nm, then the scattering signal concentrates in the central beam stop area and the measurement of gyration radius in appropriate direction is impossible. In such a case, Grubb and Prassad[20] and later Wu[21,22] proposed a method of determination of the inclusion size on the basis of the known half-width of scattering signal, analyzing the intensity profiles more and more closely to the center of the pattern. These profiles are collected in the direction from perpendicular to nonmeasurable. Half-width of the profile is approximated (not recordable) from the visible profiles in the central plane and the value is related to the size of scattering objects in the nonmeasurable direction.

The total degree of crystallinity and α and β phase content were determined using WAXS in the transmission mode, in apparatus that was equipped with a Philips generator and an X-ray lamp producing CuK_α, line. Scattered radiation was registered as a function of the angle 2θ by a scintillation counter; the measurement step was 0.05°. The objects of studies were nondeformed samples. For deformed samples a different means of crystallinity determination was applied. It is known that the results of WAXS experiment for deformed samples may strongly depend on the orientation and the best way would be to have the examined samples in the form of

TABLE I
Initial Characteristic of the Examined Samples by WAXS and SAXS Methods

Sample symbol	Processing method	Crystallinity (%)	β phase content, *K*	Long period (nm)	Long period form correlation function (nm)	Crystal thickness[a] (nm)	Thickness of amorphous layer[a] (nm)
K 90	Nucleated PP, melted and cooled in the air	58	0.90	14.5	14.2	8.4	6.1
K 73	Nucleated PP, melted and cooled in iced water	51	0.73	13.5	12.8	6.9	6.6
K 01	Non-nucleated PP, melted and cooled in the air	55	0.01	19.6	18.1	10.8	8.8

[a] Calculated from long period and crystallinity.

powder. In our case this was impossible, because the objects of interest were small parts of the examined samples. Hence, a different procedure was applied. The sample was rotated at the step of 22.5° in the plane perpendicular to the beam and 2θ diffractograms were accumulated for each position. Finally, the content of the crystalline phase was determined from an averaged diffractogram. This simplified method gives a relatively good characteristic of small volumes (i.e., 1 mm^3) of deformed polymers.

WAXS photo camera was used for observations of lamellae's orientation. A source of CuK_α radiation, operating at 50 kV and 35 mA was used. Two-dimensional scattering images were recorded by a camera equipped with a Kodak imaging plate. The distance between the sample and the recording plate was 5 cm. Exposed imaging plates were analyzed with a PhosphorImager SI system (Molecular Dynamics).

SAXS from nondeformed samples provided a source of information about the long period of structure. It was calculated from the position of the maximums on the curve $Is^2 = f(s)$; where I – intensity and s – scattering vector. The thickness of amorphous and crystalline phase were calculated from a long period and the degree of crystallinity. For the sake of comparison, the long period was also determined by the correlation function method[23–25].

RESULTS

The initial characteristic of specimens

2D WAXS examination of nondeformed PP plates did not exhibit orientation, therefore crystallinity and β phase contents were determined on the basis of diffractograms. Turner-Jones et al.[26] proposed a calculation of β phase content, *K*, from an equation:

$$K = I_{\beta(300)}/(I_{\beta(300)} + I_{\alpha(110)} + I_{\alpha(040)} + I_{\alpha(130)}) \quad (5)$$

where $I_{\alpha(110)}$, $I_{\alpha(040)}$, and $I_{\alpha(130)}$ are the integral intensities for the most intensive peaks from α phase, related to scattering from planes (110), (040), and(130), respectively. $I_{\beta(300)}$ is an integral intensity of the peak representing scattering from (300) plane of a trigonal β form. This peak is visible on a diffractogram at the angle of $2\theta = 16.2°$. The initial characteristic of our samples is presented in Table I. The applied sample symbols indicate the β phase content in the total crystallinity, for example *K* 73 means that it is 0.73.

Table I presents the influence of the preparation procedure on the β phase content. The α form crystals were dominant in the non-nucleated PP *K* 01. If a nucleant was added to a polymer and the cooling rate was slow, the highest content of β phase was obtained (*K* 90). If cooling of nucleated PP was rapid, as for *K* 73 specimen, then the β phase dominated, but also 27% of α phase was present. It can be concluded, that in the last case, due to a rapid temperature change, the superiority of β form growth rate over α form growth rate was not so significant as in the slowly cooled *K* 90 sample and more α crystals would be generated during solidification. Table I also shows that the crystallinity of the studied samples was 51–58% and it was slightly larger for the samples in which the crystallization time was longer.

SAXS provided the source of information about long periods and the thicknesses of crystals. The separation of scattering from crystal stacks of both crystallographic forms was not visible, so the data of long periods in Table I represents averaged values. The compositions rich in β phase have smaller long periods and thinner lamellae than the α phase crystals. The thinnest lamellae were generated when crystallization was rapid, i.e., for *K* 73 sample. For this sample it was not possible to separate long periods from α and β forms, which probably means that the values are similar. The thickest crystals were present in the *K* 01 sample.

Uniaxial drawing and cavitation

The mechanical behavior of drawn PP samples is presented in Figure 1(a). The yield point was

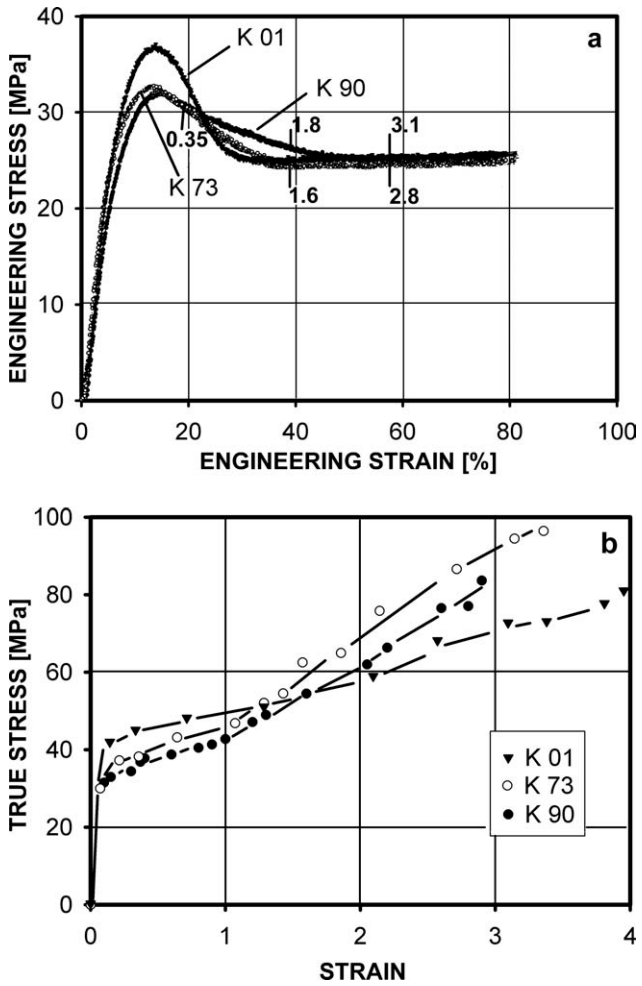

Figure 1 Engineering stress-engineering strain (a) and true stress-local strain (b) dependence for the studied materials. The numbers next to curves in (a) show the values of local strain in the most deformed parts of samples.

reached at the strain of 14–16% and the strain on yield only slightly depended on the phase content. However, the yield stress decreased with β phase content. It was 38 MPa for *K* 01 sample, 32.5 MPa for *K* 73 sample and 32 MPa for *K* 90 sample. The value of yield stress in the examined samples depended both on crystals' thickness and on the relation of phase content, which resulted in a higher stress level in *K* 73 sample than in *K* 90 sample, characterized by thicker crystals. The nonexistence of tangential lamellae in β spherulites also make deformation of *K* 90 sample easier. Figure 1(a) also presents the values of maximum local strains. They are larger than engineering strains, starting from the yield point, which indicates that deformation of PP is localized. This localization is visible in the shape of neck, formed shortly after yield. The strain localization increases slightly with β phase content.

Figure 1(b) presents the dependence of true stress on the local strain, defined by eq. (1), measured for the most deformed part of sample. One observes a continuous increase in the true stress with deformation and it is faster in the samples where β phase dominates. For the samples *K* 73 and *K* 90, a change in the line slope for the strains of 1.1–1.2 is noted. In the non-nucleated PP *K* 01 similar effect occurs for the strain of 2.0, therefore the curves intersect at the strain of 1.5. Lezak et al.[9] who studied the same polymer in the plane strain compression made a similar observation and also Xu et al.[27] who studied another PP in uniaxial compression. Xu explained that β crystals are weakly bonded in spherulites, because tangential lamellae are not present and as a result the orientation of amorphous phase occurs at lower stresses. This orientation leads to earlier strain hardening in the PP sample rich in β.

In the deformed samples, whitening occurs near the yield point. It is first visible in the most deformed part of samples and later spreads to the adjacent parts of a polymer. The whitening is illustrated in Figure 2, presenting photographs of samples before and during deformation. When the strains are large, in the range of 4–5, which is represented by the sample in Figure 2(b), the whitening area includes not only a neck, but almost the whole gauge of the sample. Figure 2 also illustrates that significant changes in measuring distances in the direction of deformation (between black marks) are accompanied by much smaller changes of perpendicular dimensions. This is especially characteristic of *K* 90 specimen. Whitening was most intensive in *K* 90 sample and least in *K* 01 sample. Usually, the reason for whitening is scattering of light on micrometer-sized voids. Because the effect is visible also at the beginning of deformation, another potential reason for whitening, additional crystallization, may be excluded. A relatively constant level of crystallinity in the examined

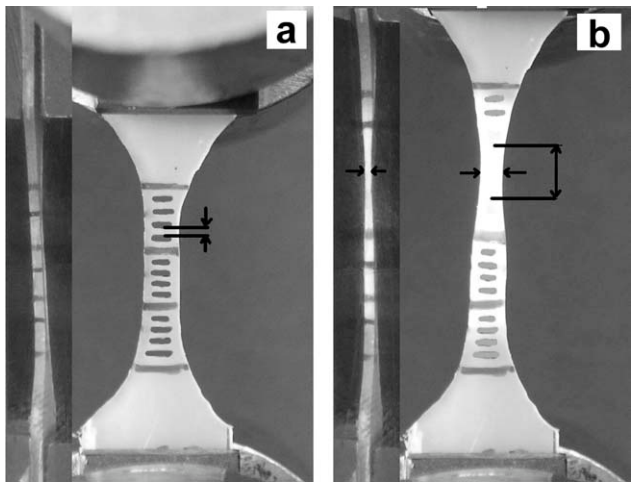

Figure 2 Sample *K* 90 photographed before (a) and during deformation (b). Whitening of the deformed sample is visible. The photo also presents the principle of determination of dimensions required for volume measurements.

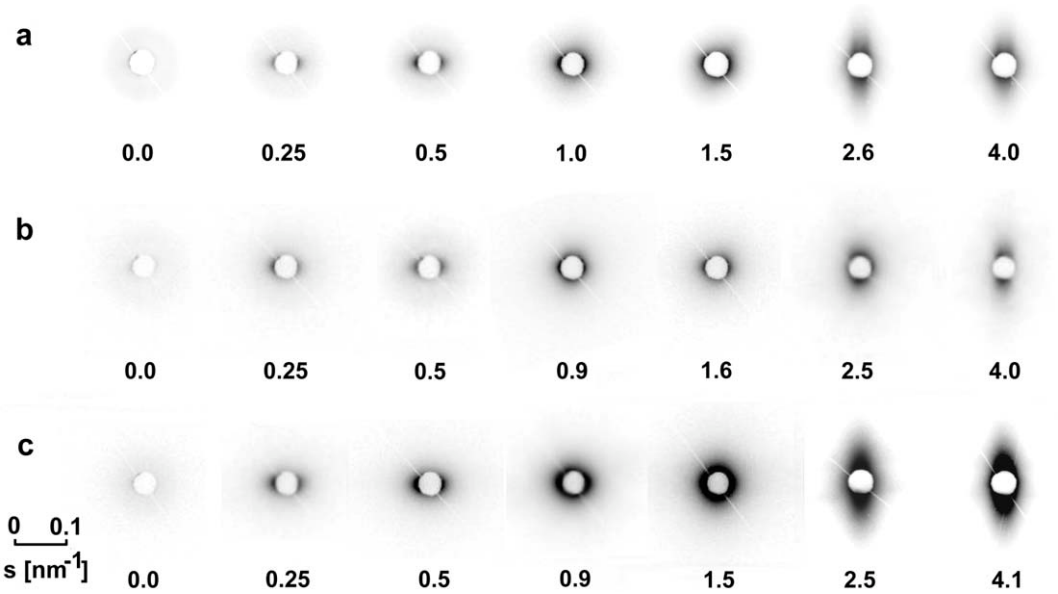

Figure 3 SAXS patterns for samples *K* 01 (a), *K* 73 (b), and *K* 90 (c). The numbers indicate local strain. The direction of deformation was horizontal.

samples was confirmed by measurements, which are discussed later.

It is known from our previous studies that in polymers together with large cavities that scatter light, also smaller, nanometer cavities are formed. These voids are detected by SAXS. The formation of nanocavities seems to be important, as being numerous they probably have a bigger influence on the deformation process than the larger ones. Figure 3 shows SAXS patterns, registered after a mechanical test for parts of the samples characterized by a different local strain. Scattering on voids is visible in SAXS patterns as black areas. The cavities were formed in all samples presented in Figure 3. The scattering on cavities is first noticed on the images for the local strain of 0.25, i.e., starting from yield point. Scattering patterns at the strain of 0.25 are elongated and oriented in the direction of deformation (horizontal), which means that cavities are ellipsoidal and elongated perpendicularly to the direction of deformation.[11,12] The lack of visible scattering in the vertical direction means that radiation is scattered inside the beam stop area, i.e., the size of cavities in the corresponding direction is larger than 40 nm.

The scattering patterns also show reorientation of cavities, occurring at the strain of 1–1.5. After reorientation, the voids are elongated in the direction of deformation. The scattering intensity increases with strain; however, the increase stops for the strains of 4.0 and larger, when some voids become so large that scattering from them begins to accumulate in the nonmeasurable central area. This is especially visible for samples *K* 01 and *K* 73.

The above discussed patterns were registered after deformation and stress relaxation. With the aim of excluding the influence of relaxation on the character of images, additional measurements were taken for selected elongations. A stressed sample was fixed in a special frame preserving the deformation state during SAXS measurements. One did not observe drastic changes in the scattering intensity or the shape of the pattern. Scattering patterns and their evolution, presented in Figure 3, are typical of cavitating semicrystalline polymers.[11,12,17]

The analysis of a scattering profile along the horizontal line (Fig. 3) allows to determine the gyration radius *R*, which is a measure of voids' size in this direction. The condition for applying Guinier's approach is that the system is diluted, with separated cavities. This seems to be accomplished at the beginning of plastic deformation, therefore *R* for samples deformed to the strain of 0.25 were determined. The results are presented in Table II. In each samples, two populations of voids are present, characterized by the gyration radii of 5 and 13 nm. The accuracy of these measurements may be estimated as ± 1 nm. However, there are significant differences in number fraction, determined by Yamashita's[19] method. The number contribution of smaller voids decreases with β phase content, from 52% for *K* 01 to only 34% for *K* 90 sample.

The radius of gyration may be directly used for determination of the voids' size, only when their shape (e.g., spherical) and orientation are known. Elongated scattering profiles indicate that cavities are, in this case, ellipsoidal. The cavities are partially oriented and probably their diameter in the direction of shorter axis of ellipsoid is for larger voids close to the thickness of amorphous layer, i.e., 6 nm. This is illustrated in Figure 4, where the sketch of probable

TABLE II
Gyration Radii and Number Participation of Groups of Cavities

Sample	Radius of gyration (nm)	Number content (%)
K 01	5	52
	13	48
K 73	5	49
	13	51
K 90	5	34
	13	66

orientation of cavities in amorphous layer, characterized by mean orientation degree of γ, is presented. Hamzeh and Bragg[28] and Bose and Bragg[29] showed the relation between R, measured in the direction of force, and half-axes a and b of ellipsoid, when the ellipsoid representing cavities is oriented under (90°-γ) angle to the direction of scattering vector. The equation has a form:

$$R^2 = (3/5) * (a^2 \sin^2 \gamma + b^2 \cos^2 \gamma) \quad (6)$$

Let us assume that: $2b = 6$ nm, $\gamma = 30°$ and $R = 13$ nm. Then, the calculation from eq. (6) shows that the length of an ellipsoid is $2a = 66$ nm, Scattering from such voids, perpendicularly to the deformation direction, would thus be outside the detection range, which agrees with the patterns presented in Figure 3. If we suppose that the smallest voids have the same elongation ratio $a/b = 11$, but more freedom of orientation, so that $\gamma = 45°$, then calculations by eq. (6) lead to the values of length of an ellipsoid: $2a = 17.6$ and $2b = 1.6$ nm.

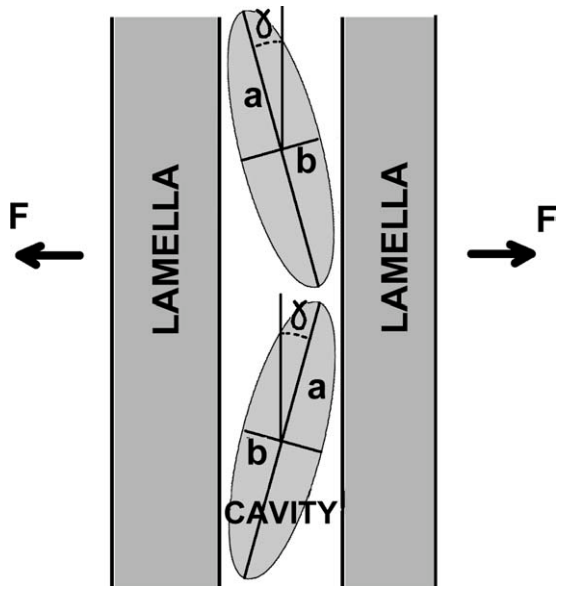

Figure 4 The sketch of cavity's location in amorphous layer.

The Guinier's equation (4) demonstrates that the participation of small and large cavities in the total scattering may be significantly different. If one takes for calculation the above dimensions and the number participation of voids (from Table II), the value of the scattering vector being $s = 2.5 \times 10^{-2}$ nm^{-1} and the volume of a single void described as $V = 4/3 \times \pi \times a \times b^2$; then it is possible to determine the ratio of scattering intensities from large and small voids. For the sample *K* 90 it is $I_2/I_1 = 32$. In the case of PP rich in α, with the same size of voids, this ratio is only $I_2/I_1 = 15$.

In most of the registered SAXS patterns, the part representing the largest dimension of void is covered by a beam-stop, therefore direct examination is impossible. However, Grubb and Prassad[20] proposed the use of a nondirect method of size determination, when scattering is not visible. Their approach to the sample deformed to the strain of 0.25 is illustrated in Figure 5. Calculations begin from large values of s, in the part of the pattern where scattering from voids is present. At the beginning, the profiles of intensity around lines in the 1–1 direction are calculated, moving toward the center of the images. An exemplary profile is presented as insertion in Figure 5.

The next step is determination of the half-width of each profile, denoted as H. When the function of H vs. s is determined, it provides the basis for approximation of the value of H at $s = 0$. Half-width H_o of the central profile 0–0 is not measurable directly. The broadening of scattering peaks is the reverse of the searched dimension L of the scattering object, and the relation is described by an equation:

$$H * \cos(2\theta)/(\lambda * D) = 1/(2L) + [1/(4L^2) + s^2 * \sin^2 \beta/(4\pi^2)]^{0.5} \quad (7)$$

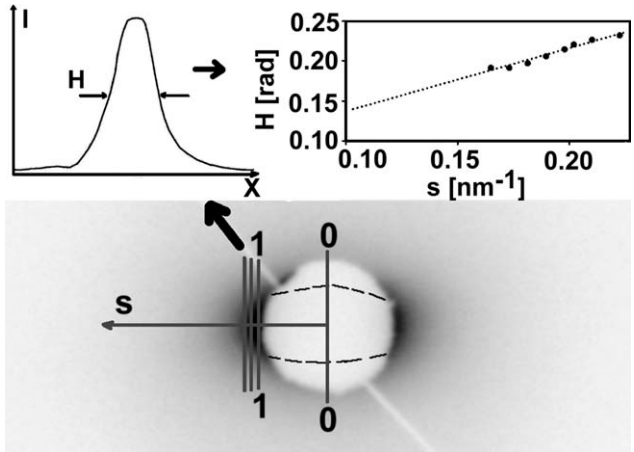

Figure 5 The scattering pattern for a sample deformed to the strain of 0.25 and the method of half-width determination for the central profile 0–0.

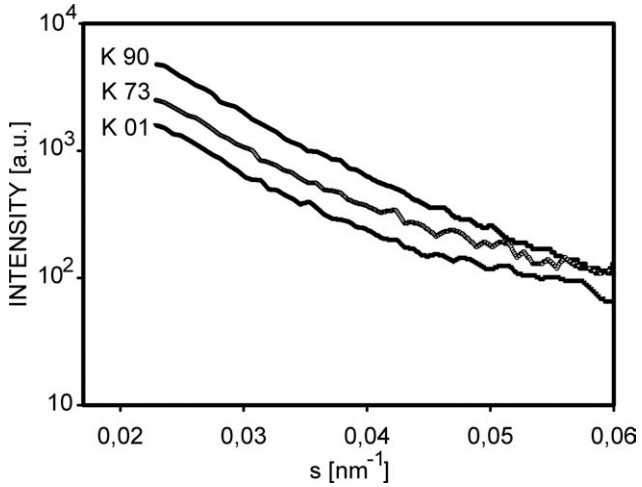

Figure 6 The intensities of small angle X-ray scattering as a function of scattering vector, determined for PP samples strained to 0.25. The profiles were taken in the horizontal direction from patterns shown in Figure 3.

where 2θ is the scattering angle, λ is the length of electromagnetic wave, D is the sample-detector distance, $s = 4\pi\sin\theta/\lambda$, and β is the orientation distribution angle. Assuming that the last term in eq. (7) is negligible and that the participation of large holes in H is the same as in the scattering intensity, it is possible to calculate the length of voids. For example, when one analyzes K 90 specimen strained to $\varepsilon = 0.25$, then the size of large holes is 63 nm. This result is close to one obtained in calculations based on the thickness of amorphous layer and gyration radius. The accuracy of Grubb–Prassad's method is limited here by a relatively large area of beam-stop, which restricts the possibility of accurate half-width determination in the position close to the center. Similar calculations made for K 01 sample gave the length of large voids equal to 66 nm.

Observations by SAXS method allows to notice another important fact – the intensity of scattering from voids increases with β phase content. It is visible in Figure 3, even if the time of registration of patterns was not the same for each sequence: 30 min for K 90, 45 min for K 73, and 90 min for K 01. Different times were selected to avoid saturation of imaging plates.

The differences between individual samples are better visible in Figure 6, presenting curves of scattering intensity as a function of scattering vector for the analyzed samples. These are horizontal scans from patterns, as in Figure 3, registered at the strain of 0.25. The curves were normalized to obtain the same time of registration and uniform thickness. It is clear from Figure 6 that the intensity of scattering on voids increases with β phase content. Because the size of cavities was similar in all samples, it means that with the increase in β phase content also the number of voids becomes larger.

In the case of the most intensively cavitating sample, K 90, the part of scattering may be attributed to larger contents of voids with $R_g = 13$ nm in relation to those with $R_g = 5$ nm. However, near a threefold increase in intensity, when comparing K 90 to K 01 sample, mainly results from an increase in the number of cavities. The scattering profiles in Figure 6 illustrate the differences in the scale of cavitation, however the best method of its presentation is a measurement of volume change.

The methodology of volume measurements during mechanical test is shown in Figure 2. The marks printed on the surface of the sample make it possible to determine local dimensions, the basis for the volume calculation. Figure 2(a) shows the K 90 sample before the experiment and Figure 2(b) the same sample when the local strain was around 5. The measured volume (limited by horizontal marks and edges of the sample) increased significantly. Figure 7 presents evolution of volume with deformation for all analyzed samples. The volume strain was determined for the mostly deformed part of each sample. Figure 7 shows that the volume increases with deformation for all samples. Initially, to the strain of 0.3, the increase nearly does not depend on the β phase content. For larger strains the differences between samples are visible. The volume of K 01 sample increases to the strain of 1.0, where it is $\Delta V/V_o = 0.35$, but later the volume of the sample remains approximately constant. The volume of K 73 sample increases 0.4 for the strain 1.0, however in this case the further increase in volume was observed for larger strains. The maximum value of 0.8 corresponds to the strain of 3.5. When this sample was deformed further, the volume remained constant.

The increase in volume was very fast in K 90 specimen. At the strain of 1.0 the volume change was 0.65. The increase in volume was linear for larger strains, with the change of slope at $\varepsilon = 1.5$, i.e.,

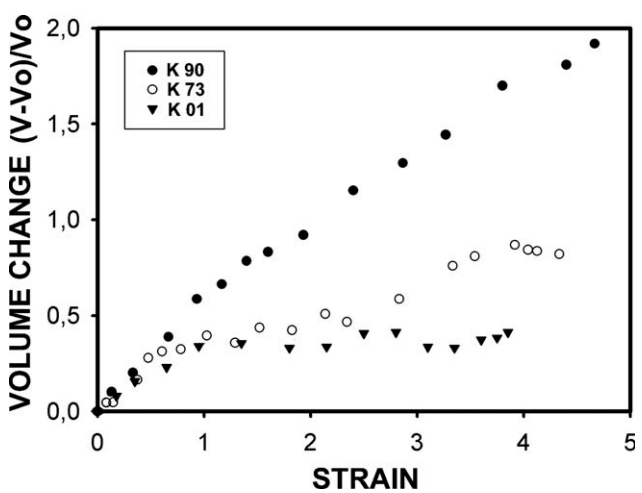

Figure 7 Volume strain in deformed PP samples.

approximately at the moment when the neck is already formed and begins to propagate.

The largest volume strain was determined for *K* 90 sample, deformed to the strain of 5 and it was $\Delta V/V_o = 1.9$. In the cavitating crystalline polymers one usually observed an increase in volume not more than 0.5–1.0.[5,11,12] Such a large increase as in the case of β-rich PP is noticed for the first time. In the semicrystalline polymers, nearly all of the increase in volume during uniaxial deformation may be attributed to the formation of cavities. The character of volume change with deformation and with β phase content agrees with SAXS observations of cavitation (Figs. 3 and 6) and with the observations of whitening, which confirms the reason for the observed changes. The character of volume change in sample *K* 73 is closer to the curve representing *K* 01 sample than it would be expected from β phase content only. However, this sample was solidified by cooling in iced water, which, as known from previous experiments,[12] partially reduces the ability to cavitation and due this also reduces the increase of volume.

In principle, the volume strain $w = \Delta V/V_o$ may have three components: elastic, cavitational, and plastic, the last one representing the noncavitational modes of plastic deformation. If the last factor is omitted, then the following relationship is true:

$$\Delta V = \Delta V_e + \Delta V_h \tag{8}$$

where ΔV_e is the elastic component, and ΔV_h is the cavitational component of the volume change. The elastic component may be described as:

$$\Delta V_e = V_o(1 - 2\nu)\varepsilon \tag{9}$$

where V_o is the initial volume of amorphous layer, ν – Poisson coefficient, and ε – strain. The equation describing cavitational component has a form:

$$\Delta V_h = N * \sum_{i=1}^{M} (n_i * 4/3 * \pi * a_i * b_i^2) \tag{10}$$

where N is the total number of voids in the volume V_o, n_i – number fraction of voids, a_i and b_i – half-axes of ellipsoids describing voids' shape, and M – the number of different void populations. If only two groups of cavities exist in a polymer, then by combining eqs. (8)–(10), a new equation is formed, which allows to calculate the number of voids N:

$$N = V_o * [w - (1 - 2\upsilon)\varepsilon]/[4/3 * \pi * (n_1 * a_1 * b_1^2 + n_2 * a_2 * b_2^2)] \tag{11}$$

The typical structure in the microscale of our samples is that the crystalline lamellae are separated by amorphous layer. Let us assume that the volume V_o consists of one crystalline and one amorphous layer, with the length of 1000 nm. According to Table I, the thickness of lamella in *K* 90 sample is 8.4 nm and the thickness of amorphous layer 6.1 nm. The width of lamella-amorphous layer assembly may also be taken as 6.1 nm. At the strain of $\varepsilon = 0.25$ the volume change in our sample was $w = 0.15$ (see Fig. 7). The analyzed PP is characterized by the Poisson coefficient $\nu = 0.36$. Another assumption is that large, micrometer voids are not numerous at that moment and may be omitted in calculations. If our material is *K* 90 PP, then according to Table II the contributions of nanovoids are $n_1 = 0.34$ and $n_2 = 0.66$. Their dimensions may be taken as previously: $a_1 = 8.8$ nm, $b_1 = 0.8$ nm, $a_2 = 33.0$ nm, and $b_2 = 3.0$ nm. Introduction of these data into eq. (11) gives the number of voids $N = 8.5$. It means that the average distance between the centers of cavities, which are located only in the amorphous layer, is around 150 nm. The calculation for *K* 01 sample may be done using the same values, with the exception of $w = 0.12$, $n_1 = 0.52$, and $n_2 = 0.48$. In this case, the number of voids calculated from eq. (11) is $N = 7.2$, i.e., the distance between cavities is here slightly larger.

The above evaluations demonstrate that more than one cavity may be present near the surface of lamella. Similar calculations are impossible for larger strains, because many assumptions, e.g., Guinier's concerning not interacting cavities, may not be fulfilled.

Cavities are generated in the amorphous phase between lamellae. As a result, the observed changes in shape depend on reorganization and reorientation of the surrounding polymer. The efficient tool for the study of evolution of crystalline structure is wide-angle X-ray scattering. Figure 8 presents two-dimensional patterns registered for the examined PPs. The images were registered after a mechanical test in the selected locations in the gauge of samples, in which the strain reached during deformation was known.

Figure 8(a) shows a sequence of scattering patterns for the sample *K* 01, which has many α crystals. The rings, starting from the center, represent diffraction on the crystallographic planes: (110), (040), (130), and (111) together with (−131) and (041). The orientation of crystals is not observed at the beginning of deformation. It does not necessarily mean that the lamellae do not change their positions at small strains, because the existing interlamelar slips may compensate for the rotation of lamellae as a whole, therefore the orientation of the diffraction planes does not change.[17]

The orientation of planes is first visible, when the strain reaches 1.4. Then, the diffractions on planes (110), (040), and (130) concentrate in the direction

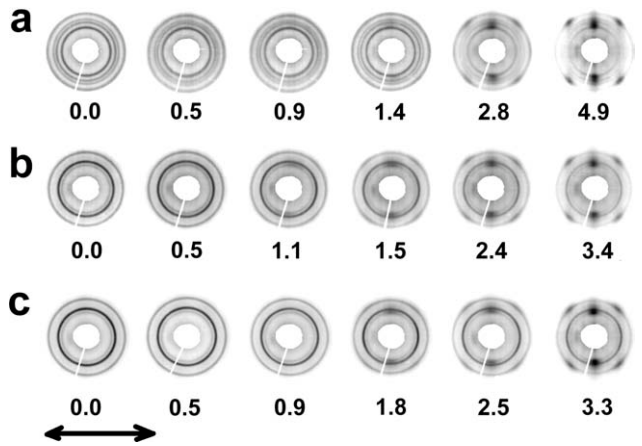

Figure 8 Wide angle X-ray scattering patterns for the samples *K* 01 (a), *K* 73 (b), and *K* 90 (c). The direction of deformation was horizontal. Numbers indicate strain values.

perpendicular to deformation. These planes contain macromolecular chains, so the change of scattering pattern indicates the progressive orientation of a polymer. Because the strain of 1.4 four maxima on the outer ring are visible, located at around 30°, relating to deformation direction. They are result of diffraction from the planes (111), (−131), and (041) of lamellae oriented in the deformation direction. Previous studies (see Fig. 7) showed that at strain of 1.4 the volume increase of sample saturates and the neck begins to propagate. The scattering patterns for strains of 2.8 and 4.9 show that the orientation of specimen increases with strain. For large strains additional scattering in the vertical direction, located between rings, is visible in the pictures, which indicates the presence of smectic phase. In the studied PP the smectic phase was formed after reorientation of voids.

Figure 8(b,c) presents scattering images for samples containing more of the β phase. Three concentric rings are clearly visible. The two inner ones represent scattering on planes (110) of α crystals and (300) of β crystals. Outside the two rings there is a weak ring representing the scattering on plane (040) of α form. The third strong ring is from diffraction at the angle $2\theta = 21.1°$. It contains mixed scattering from planes (301) of β form (at $2\theta = 21.1°$) and (111) of α form (at $2\theta = 21.3°$). The intensities from other planes are very small. In the identification of scattering planes of β form indexing based on the unit cell containing nine polymer chains was used. Some authors also apply identification based on trigonal three-chain unit cell. In this indexation the plane (110) is equivalent to the plane (300) and (111) plane is equivalent to (301).[10]

The photographs in Figure 8(b) show that the isotropic scattering is preserved in sample *K* 73, up to the strain of 1.0. When the strain is larger, the orientation of α crystals occurs, which is visible as a concentration of signals from (110) planes in the vertical direction. Simultaneously, at the strain of 1.5, the formation of four maxima is visible in the outer ring, probably also due to orientation of α crystals. The ring which represents scattering form (300) planes of β form is uniform even for large deformations. When strains are large (i.e., 2–3), one observes additional scattering from planes parallel to the direction of deformation, located vertically between two outer rings, for angles in the range $2\theta = 14–16°$. The scattering is probably a result of orientation of a polymer in the amorphous phase and formation of smectic phase. Figure 8(c) shows that the structural changes in *K* 90 sample occur similarly to *K* 73. The scattering from α crystals is here less intensive, because their content is lower in the *K* 90 sample.

It must be noted that the uniformity of the ring representing (300) plane of β phase was preserved even for the largest strains. Similar observations, stating that the orientation of crystalline planes does not occur for small and intermediate strain, were earlier made by Riekel and Karger-Kocsis.[7] The reason for this may be that chain slips, which compensate for the effect of lamellar rotation under stress, are more easily initiated in β crystals oriented diagonally than in α crystals. The nonexistence of crystal orientation up to the large strain ratio may influence the continuity of voids generation in the samples rich in β form.[7]

The analysis of X-ray diffractograms registered for *K* 90 specimen before the mechanical test and after deformation to strain $\varepsilon = 3.0$ showed that the total crystallinity decreases due to deformation from 58% to 52%. The diffractogram used for determination of crystallinity after straining was averaged from measurements at different directions, as previously discussed. Reflections from different crystalline planes and contributions of phases were separated by applying Optifit software.[30] The *K* coefficient did not change, which means that the possible transformation β →α did not occur. The content of the newly formed smectic phase was about 5%.

CONCLUSIONS

The tensile test showed that the examined PPs deformed with the formation of neck. The stress at yield decreased when the β phase content was larger, which was the result of thinner lamellae of β form, nonexistence of tangential lamellae and lower strength of β form crystals.[9] Localization of deformation, measured as a function of local strain vs. engineering strain [Fig. 1(a)], was a little bit more pronounced in the samples rich in β form. Cavitation occurs in deformed PPs and begins at yield.

Voids were detected by SAXS, because their sizes were in a nanometer range. When the strain increased the samples whitened, which was an evidence of generation of larger cavities, of micrometer size (Fig. 2).

SAXS experiment enabled to determine the size and shape of cavities and their evolution during an increase in deformation. Cavities, irrespective of crystalline form of samples, were initially elongated perpendicularly to the direction of deformation. Change of shape of cavities, i.e., orientation toward the direction of deformation occurs at the local strain of 1.5. Reorientation of voids was forced by the change in lamellas' orientation and subsequent progressive transformation of lamellar structure into the oriented fibrillar structure. This can be partly confirmed by the evolution of WAXS images for α form, indicating orientation of macromolecular chains in the direction of deformation. Similar orientation effects were not observed in WAXS patterns of β form PP, which may result from more intensive interlamellar slips, compensating for crystal rotation.

The analysis of SAXS patterns showed that two populations of nanosize voids exist in the examined samples and that voids have the same dimensions irrespective of the content of β phase in the studied sample. This may partly result from similar thickness of amorphous layers, which was 6.1 nm for *K* 90 and 8.8 nm for *K* 01. The intensity of SAXS depends on the β phase content in the sample, which indicates that cavitation is much more intensive in the presence of β crystals. The newly generated voids probably promote deformation of β spherulites, which results in stronger localization of plastic deformation, observed in β rich samples.

The scale of cavitation is best characterized by the measurements of volume strain, because practically the entire increase in volume results from voiding. In all cases, the increase in volume is significant. It depends on the β phase content and when these type of crystals dominate in a sample, it may even be 200% of the initial volume, as observed for *K* 90 sample strained to 5.0.

The existing methods do not allow for exact determination of the size of voids and the number of cavities per volume of the deformed material. The calculations based on SAXS measurements for the strain of 0.25, i.e., for the beginning of plastic deformation, gave the values of length and width of two populations of voids as 58–66 nm and 6 nm for larger voids and length of 18–22 nm, width of 2 nm for smaller voids. The estimated distance between the centers of voids in amorphous layer was at this strain around 150 nm, which shows that typically there exist more than one cavity near the lamellar surface. The presence of voids modifies the local state of stress, which may intensify the deformation processes, such as fragmentation of lamellae.

References

1. Seguela, R.; Staniek, E.; Escaig, B.; Fillon B. J Appl Polym Sci 1999, 71, 1873.
2. Kotek, J.; Kelnar, I.; Baldrian, J.; Raab, M. Eur Polym J 2004, 40, 670.
3. Varga, J.; Ehrenstein, G. W. In Polypropylene. An A-Z reference; Karger-Kocsis, J., Ed.; Kluwer Academic Press: Dordrecht, 1999; p 51.
4. Aboulfaraj, M.; G'Sell, C.; Ulrich, B.; Dahoun, A. Polymer 1995, 36, 731.
5. Shi, G.; Chu, F.; Zhou, G.; Han, Z. Die Makromol Chem 1989, 190, 907.
6. Li, J. X.; Cheung, W. L. Polymer 1998, 39, 6935.
7. Riekel, C.; Karger-Kocsis J. Polymer 1999, 40, 541.
8. Chu, F.; Yamaoka, T.; Ide, H.; Kimura, Y. Polymer 1994, 35, 3442.
9. Lezak, E.; Bartczak, Z.; Galeski, A. Polymer 2006, 47, 8562.
10. Lezak, E.; Bartczak, Z. Fibres Textile Eastern Eur 2005, 13, 51.
11. Pawlak, A.; Galeski, A. Macromolecules 2005, 38, 9688.
12. Pawlak, A.; Galeski, A. Macromolecules 2008, 41, 2839.
13. Pawlak, A. Polymer 2007, 48, 1397.
14. G'Sell C., Hiver J. M., Dahoun A. Int J Solids Struct 2002, 39, 3857.
15. Addiego F., Dahoun A., G'Sell C., Hiver J. M. Polymer 2006, 47, 4387.
16. Schneider K., Trabelsi S., Zafeiropoulos N. E., Davies R., Riekel Ch., Stamm M. Macromol Symp 2006, 236, 241.
17. Pawlak, A.; Galeski, A. J Polym Sci Part B: Polym Phys 2010, 48, 1271.
18. Guinier, A. Ann Phys 1939, 12, 161.
19. Yamashita, T.; Nabeshima, Y. Polymer 2000, 41, 6067.
20. Grubb, D. T.; Prassad, K. Macromolecules 1992, 25, 4575.
21. Wu, J. Polymer 2003, 44, 8033.
22. Wu, J.; Schultz, J. M.; Yeh, F.; Hsiao, B. S.; Chu, B. Macromolecules 2000, 33, 1765.
23. Strobl, G. R.; Schneider, M. J Polym Sci Polym Phys Ed 1980, 18, 1343.
24. Goderis, B; Reynaers, H.; Koch, M. H. J.; Mathot, V. B. F. J Polym Sci Part B: Polym Phys 1999, 37, 1715.
25. Janicki, J.; Rabiej, S.; Wlochowicz, A. Polimery 2004, 49, 248 (in Polish).
26. Turner-Jones, A.; Aizlewood, J. M.; Beckett, D. R. Macromol Chem 1964, 75, 134.
27. Xu, W.; Martin, D. C.; Arruda, E. M. Polymer 2005, 46, 455.
28. Hamzeh, F. M.; Bragg, R. H. J Appl Phys 1974, 45, 3189.
29. Bose, S.; Bragg, R. H. J Appl Phys 1978, 49, 2916.
30. Rabiej, M.; Rabiej, S. Fibres Textiles Eastern Eur 2005, 13, 75.